Article

Multibody Simulation for the Vibration Analysis of a Turbocharged Diesel Engine

Enrico Armentani [1,*], Francesco Caputo [2], Luca Esposito [3], Roberto Citarella [4]

[1] Dept. of Chemical, Materials and Production Engineering, University of Naples Federico II, P.le V. Tecchio, 80, 80125, Napoli, Italy; enrico.armentani@unina.it
[2] Dept. of Engineering, University of Campania "Luigi Vanvitelli", Via Roma, 29, 81031 Aversa (CE), Italy; francesco.caputo@unicampania.it
[3] Dept. of Industrial Engineering, University of Naples Federico II, P.le V. Tecchio, 80, 80125, Napoli, Italy; luca.esposito2@unina.it
[4] Dept. of Industrial Engineering, University of Salerno, Via Giovanni Paolo II, 132, Fisciano (SA), Italy; rcitarella@unisa.it
* Correspondence: enrico.armentani@unina.it; Tel.: +39-081-768-2450

Abstract: In this paper, a multibody calculation methodology has been applied to the vibration analysis of a 4-cylinder, 4-stroke, turbocharged diesel engine, with a simulation driven study of the angular speed variation of a crankshaft under consideration of different modeling assumptions. Moreover, time dependent simulation results, evaluated at the engine supports, are condensed to a vibration index and compared with experimental results, obtaining satisfactory outcomes. The modal analysis also considers the damping aspects and has been conducted using a multibody model created with the software AVL/EXCITE. The influence of crankshaft torsional frequencies on the rotational speed behavior has been evaluated in order to reduce the vibration phenomena.

Keywords: Vibration analysis, FEM, Multibody.

1. Introduction

Structural and acoustic modelling methods, used to predict the performance of car and aerospace components in terms of noise and vibration, have become the key tools in the design process [1].

The car engine dynamics is explored especially in the low frequency range and at low engine speeds, where the direct vibration transmission by the engine mounts is a critical excitation mechanism, whereas, rising the maximum analyzed frequency constitutes an important industrial challenge for automotive and aerospace industry [2].

There are several examples in literature describing a combination of multi-body simulation, including flexible FE subsystems, to perform dynamics and acoustic simulation of mechanical components.

In [3], a multibody model of a car engine valve train system was developed, in order to analyze its resonant vibrational behavior. The dynamics of the valve train system was analyzed, applying a ramp to the crankshaft with a variable engine speed and considering the motion unsmoothness deriving from the inertia and combustion pressure loads.

In [4] the development of a numerical model to predict noise radiated from manual gearboxes due to gear rattle is provided. The measured data is used to identify and reproduce the input excitation which is primarily generated from engine combustion forces. The dynamic interaction of the gearbox components, including flywheel, input/output shafts, contacting gear-pairs, bearings, and flexible housing is modelled using flexible multibody techniques. The acoustic response to the vibration of the gearbox housing is then predicted using vibro-acoustic techniques.

Peer-reviewed version available at Appl. Sci. 2018, 8, 1192; doi:10.3390/app8071192

In [5-6] the numerical modelling of noise radiated by an engine and by a car body respectively, using the so-called Acoustic Transfer Vectors and Modal Acoustic Transfer Vectors concepts, is presented. The dynamics of the engine are described using a finite element model loaded with an RPM-dependent excitation.

In [7], a technique to compute the noise radiated by a large truck engine is presented: the vibration is computed using a commercial FEM code, whose results are subsequently used in an acoustic radiation computation.

In [8], a vibro-acoustic numerical and experimental analysis was carried out for the chain cover of a low powered four-cylinder four-stroke diesel engine. A boundary element (BE) model of the chain cover was realized to determine the chain cover noise emission, starting from the previously calculated structural vibrations. The numerical vibro-acoustic outcomes were compared with those experimentally observed, obtaining a good correlation.

In [9-10], a novel and effective mathematical models and advanced analytical approaches to achieve more accurate prediction of spiral bevel gear dynamic response were developed to investigate the underlying physics affecting gear mesh and gear dynamic response generation and transmissibility.

In [11] an in-depth investigation on the dynamical load sharing behaviors of a four-planetary gear system with multi-floating components was provided.

In [12] the impact of coupling engine structure with rotating components on the engine noise and vibrations across all rpm and frequency range is illustrated.

The need for accurate models forms a major obstacle to the implementation of cylinder balancing methods for engines with a high number of cylinders [13]. This is due to closely spaced cylinder firings and the fact that the crankshaft dynamics cannot be ignored, partly due to the increased length of the crankshaft, and partly because analysis of higher frequency components is required to obtain sufficient information for balancing the cylinder-wise torque contributions. This deformation can assume significant values depending on the engine-load configuration (load change, crankshaft stiffness, kind of aspiration of the engine), and as such it is of great importance for safe engine operation.

In [14], an experimentally validated diesel engine simulation code is used to study and evaluate the importance of a notable engine dynamic issue, i.e. the crankshaft torsional (angular) deformations during turbocharged diesel engine operation, owing to the difference between instantaneous engine and load (resistance) torques. The analysis aims ultimately in studying the phenomena under the very demanding, and often critical, transient operating conditions. Details are provided concerning the underlying mechanism of the crankshaft torsional deformations during steady-state and transient operation.

In [15] a methodology for predicting the piston to liner contact in running engines by means of MBD (Multi-Body Dynamics) and FEM is presented. In addition to the mathematical modelling of the excitation the paper describes the transfer mechanisms of the piston slap phenomenon. Thus, the model is extended in order to analyze vibration transfer via engine structure. Results of simulation work show structure surface velocity levels and their contribution to integral levels in different frequency bands.

In [16] the mathematical modelling of body structures and the calculation of the non-linear connecting forces resulting from elastohydrodynamic contacts between piston-liner or shaft-bearing is described. Results of parametric studies, e.g. the influence of piston surface profile on the contact mechanism between piston and liner, are shown.

In [17] CAE capabilities in the simulation of the dynamic and acoustic behavior of engine, with focus on the relative merits of modification and full-scale structural/acoustic optimization of engine, is presented.

In [18] an investigation of the diesel engine combustion-related fault detection capability of crankshaft torsional vibrations is presented: the torsional vibration amplitudes are used to superimpose the mass and gas torque; further mass and gas torque analysis is used to detect fault in

Preprints (www.preprints.org) | NOT PEER-REVIEWED | Posted: 16 May 2018 doi:10.20944/preprints201805.0223.v1

Peer-reviewed version available at Appl. Sci. 2018, 8, 1192; doi:10.3390/app8071192

the operating engine. The engine dynamics is analyzed with a focus on the low frequency range and at low engine speeds, when the vibration transmission through engine mounts becomes critical.

In [19-20] a detailed multi-body numerical model of an engine prototype was used to characterize the whole engine dynamic behavior, in terms of forces and velocities. A combined usage of FEM and multi body methodologies were adopted for the dynamic analysis: both crankshaft and cylinder block were considered as flexible bodies, whereas all the other components were considered as rigid.

2. Problem Description and Modelling Approach

The problem analyzed concerns a numerical study of the vibrations of an in-line 4-cylinder, 4-strokes, internal combustion turbocharged diesel engine, to be used as a first step for future vibroacoustic analyses. Instead of a complex numerical analysis of the system through a direct finite element method which could involve prohibitive number of degrees of freedom, the authors present a modelling approach exhibiting gradually increasing complexity, starting from rigid body analysis and introducing progressively the elastic behavior of the various subsystems, using then finite element modelling with a modal analysis. The originality of the overall approach is that it combines, for a very complex system, the various numerical approaches with an experimental analysis of the system.

The analyses are focused on the 2nd, 4th, 6th and 8th order of motion irregularities which are analyzed at the flywheel and pulley. In addition, the time dependent simulation results at the engine support brackets (engine bracket, gearbox bracket and differential bracket) are evaluated, condensed to a vibration index and finally compared with experimental results.

A Multi-Body Dynamic Simulation (MBDS) of the crank train was used to characterize its dynamic behavior, starting from engine geometrical data and the available combustion loads, with both mechanical and combustion forces acting simultaneously on the crankshaft.

In order to examine the vibration behavior of the considered internal combustion engine, the behavior of the crankshaft was specifically analyzed with a focus on its torsional vibrations, namely calculating the motion irregularities of the crankshaft itself.

For the issue at hand the modeled components were: crankshaft, pistons, connecting rods, main and conrod bearings, engine mounts (also named “support brackets”), contact stiffness between piston and cylinder.

The first realized model assumed rigid bodies, allowing to assess the course of the motion irregularities of the crankshaft at low frequencies (typically those not sufficiently high to trigger the first torsional frequency).

The next step was the introduction of a crankshaft flexible model, leveraging on a Finite Element Analysis (FEA), in order to evaluate more accurately its dynamic behavior at higher frequencies; the frequency range of interest was anyway limited to the low-medium frequencies because the whole engine is modelled as rigid with the only exception of crankshaft.

Subsequently, the crankshaft FE model was further refined taking into consideration the presence of another component, the clutch: this allowed to obtain more accurate outcomes with reference to support brackets vibrations.

Finally, a numerical-experimental correlation for the validation of the numerical model was carried out.

Hypermesh and Abaqus [21] codes were respectively used for the FE modeling and modal analysis, whereas the realization of the multibody model and the forced vibrations analysis was demanded to AVL / Excite code [22].

The multibody code considers the behavior of individual bodies as linear elastic; such bodies can be subject to both large rigid body motions and small deformations.

The applied external forces come from the pressure cycle (Fig. 1) of the combustion gases [23]. All the forces of inertial nature are calculated internally by the code according to the actual speeds and accelerations of the bodies. The calculation performed for each operating regime and in the time

Preprints (www.preprints.org) | NOT PEER-REVIEWED | Posted: 16 May 2018 doi:10.20944/preprints201805.0223.v1

Peer-reviewed version available at Appl. Sci. 2018, 8, 1192; doi:10.3390/app8071192

domain provides the displacement, speed and acceleration time histories of all the points of the system.

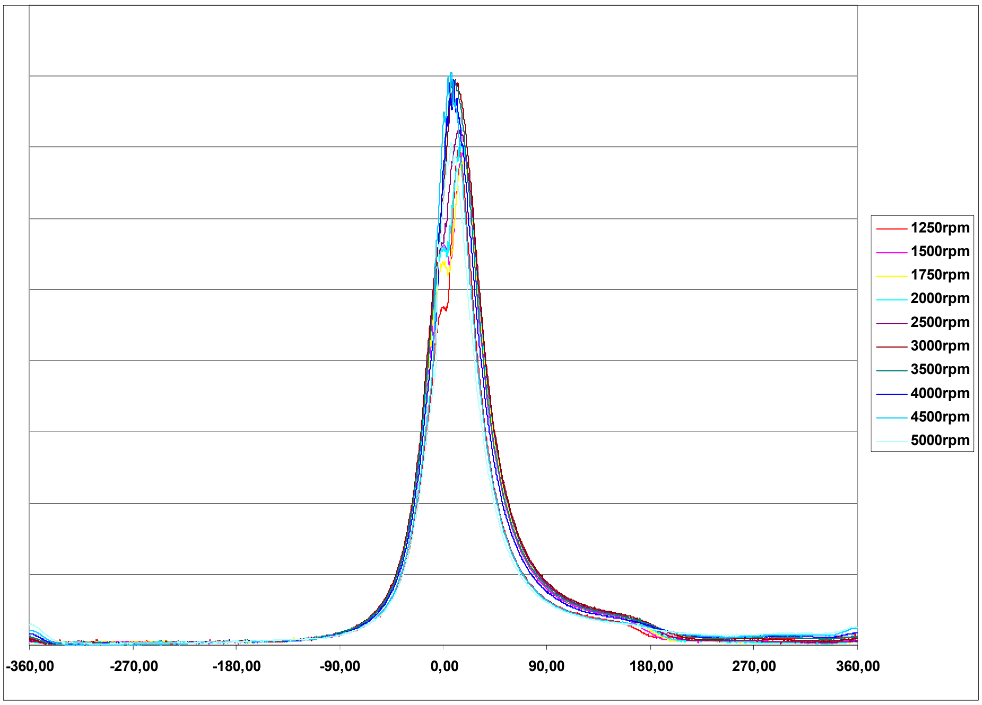

Figure 1. Experimental pressure cycles at different regimes for the engine under analysis.

2.1. System dynamic reduction

It was first built a finite element model, then, through Craig Bampton condensation [24], the appropriate mass and stiffness matrices, which are the input for the multibody software, were determined. The result of this operation turns out in a much smaller number of degrees of freedom with respect to the starting model, but still with a dynamic response that is nearly identical to that of the complete model, in the range of the frequencies of interest. In particular, the first 50 eigenforms are used for the modal reduction (such number is judged sufficient for the scope), as provided by a natural frequency extraction with constraint retained static dofs (Lanczos resolution method).

The eigenvectors are normalized by the system modal mass.

The discrepancy between the natural frequencies of the reduced model and those of the original model is corrected when the flexible body is connected, through the various joints, to the other bodies included in the overall excite model. As a matter of fact, after the assembly of the global model and after the conversion from Abaqus to Excite, setting the option

"create model" it is possible to check if the natural frequencies of the single body (reduced model) match with the natural frequencies coming from the modal analysis of the complete model.

The concept underlying the creation of a multibody model is to subdivide a mechanical system, having an overall nonlinear elastic behavior, into linear elastic sub-systems and to concentrate nonlinearities in the connections between them. The elastic bodies are represented by the condensed matrices of the corresponding FE model. Each elastic body is discretized by a number of nodes, usually those chosen in condensation, having a mass and connected to each other by massless springs and dampers. In this way, a sub-body is identified between two nodes. The interaction between the large rigid body motions and the small displacements is simulated by means of different reference systems: a global reference system S, a reference system S' integral with the body and whose origin is in the center of gravity of the body itself, and a reference system S'' integral with the considered sub-body. If the whole body were rigid each single sub-body motion, with respect to

Preprints (www.preprints.org) | NOT PEER-REVIEWED | Posted: 16 May 2018 doi:10.20944/preprints201805.0223.v1

Peer-reviewed version available at Appl. Sci. 2018, 8, 1192; doi:10.3390/app8071192

the reference system S', would be represented by null displacements and velocities. This means that vibrational outcomes of an elastic body are obtained with respect to the reference system S'.

Each sub-body belonging to an elastic body is subject to external forces and moments, deriving from the interaction with the adjacent sub-bodies and/or with the outside. Their motion is governed by the Impulse-momentum theorem, moment-of-momentum theorem and angular momentum theorem that, when enforced, provide a system of matrix equations, based on the assessment of masses, damping and stiffness matrices, applied forces and moment vectors, constraint reactions and generalized displacements.

In Figure 2 the schematization of the constraints and components making up the engine are shown (Fig. 2a), with highlight of condensation nodes of the flexible crankshaft (Fig. 2b).

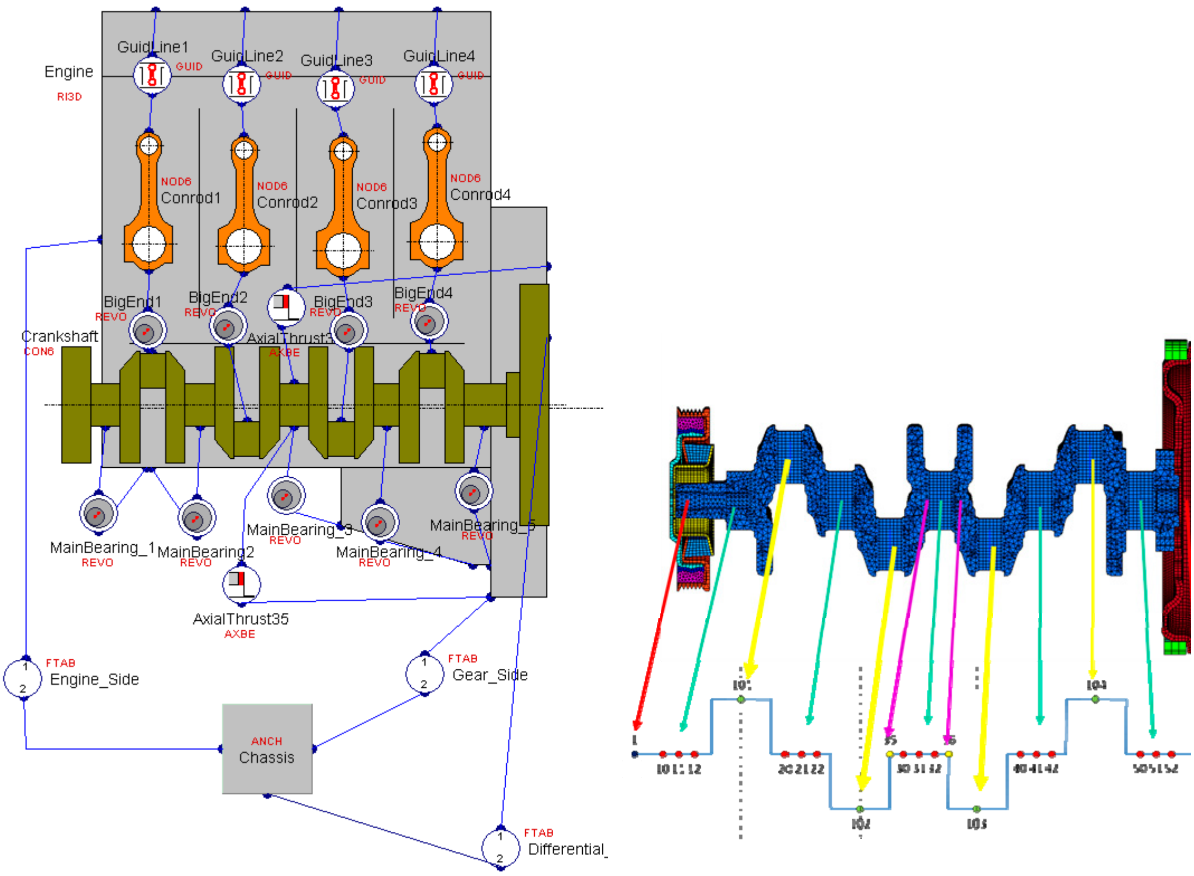

Figure 2. Graphic representation of bodies and connections (**a**) and highlight of crankshaft points used as master-nodes for the reduction process (**b**).

For the damping matrix, the multibody software refers to the so-called 'proportional damping', known as “Rayleigh damping” (Fig. 3), usually adopted when considering solid bodies (the crankshaft in this case) for which the viscous damping is not precisely known. Its expression is given by a linear combination of mass and stiffness matrices.

Peer-reviewed version available at Appl. Sci. 2018, 8, 1192; doi:10.3390/app8071192

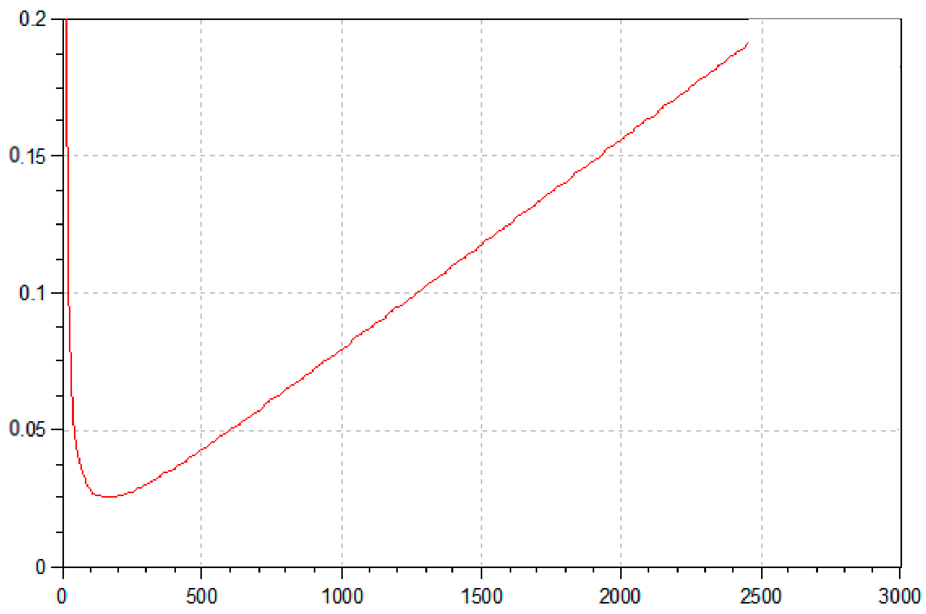

Figure 3. Rayleigh damping vs frequency (Hz) for the crankshaft.

The equations solved by AVL / Excite result in the vibrational outputs of the single elastic bodies and the characteristics of the global motion of the whole system. The solution of the equations of motion is of course subject to the input data, i.e. the external forces and all the constraint conditions necessary to the model characterization.

Those engine components considered as elastic bodies (e.g. the crankshaft) are characterized by mass and stiffness matrices containing geometric and physical information.

2.2. Models of increasing complexity

For the analysis of the vibration behavior of the internal combustion engine under examination, three models of increasing complexity were realized:

- the first, called SOL1, realizes the simulation of the engine behavior using a rigid body model (Fig. 4) and provides for the trend of the motion irregularities at low frequencies with a first evaluation of the vibrations of the power train support brackets. The powertrain suspension brackets in the engine compartment are three: engine bracket, differential bracket, gearbox bracket (Fig. 5a-d). These components are usually simulated in AVL/Excite as joints and treated as massless material points. The joints simulating the brackets were of Table Force/Moment type. This constraint allowed to introduce the nonlinear behavior of the dowels stiffness's; stiffness and damping values were assigned (as retrieved from FCA database) in the three directions x, y, z for each bracket and for different relative displacement values. The stiffness and damping values for the power train mounts were provided by the supplier through a nonlinear relation between stiffness/damping and mount deformation.
- The second model, called SOL2, is based on the FE modeling of the crankshaft, with pulley and flywheel, in order to consider the flexibility of the crankshaft that, once appropriately condensed, is introduced into the multibody calculation code and provides the values of the motion irregularities also at higher frequencies, in addition to the support brackets vibrations. Comparing Figure 6 and Figure 2b it is possible to see an added condensation node (N.2) as requested by the splitting of pulley in two independent parts (capable of relative motion), the first (node N.1) referring to the shaft end and the second (node N.2) referring to the seismic mass. Now it is possible to point out the impact of torsional modes (in case they are excited) on the motion irregularities and support bracket vibrations and this will be analyzed in the next paragraph.
- The third model, called SOL3, shows the FE modeling for both the crankshaft previously considered and the clutch unit.

Preprints (www.preprints.org) | NOT PEER-REVIEWED | Posted: 16 May 2018 doi:10.20944/preprints201805.0223.v1

Peer-reviewed version available at *Appl. Sci.* **2018**, *8*, 1192; doi:10.3390/app8071192

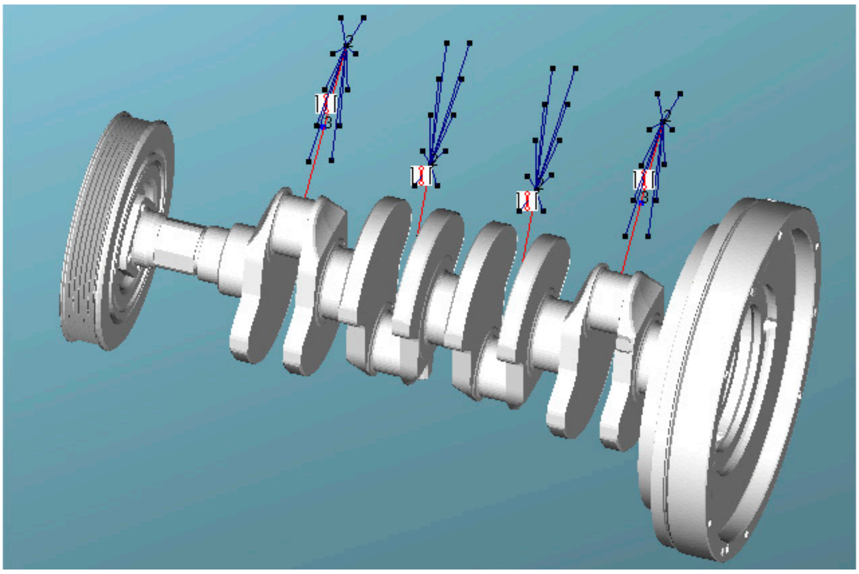

Figure 4. Crank train with highlight of force introduction.

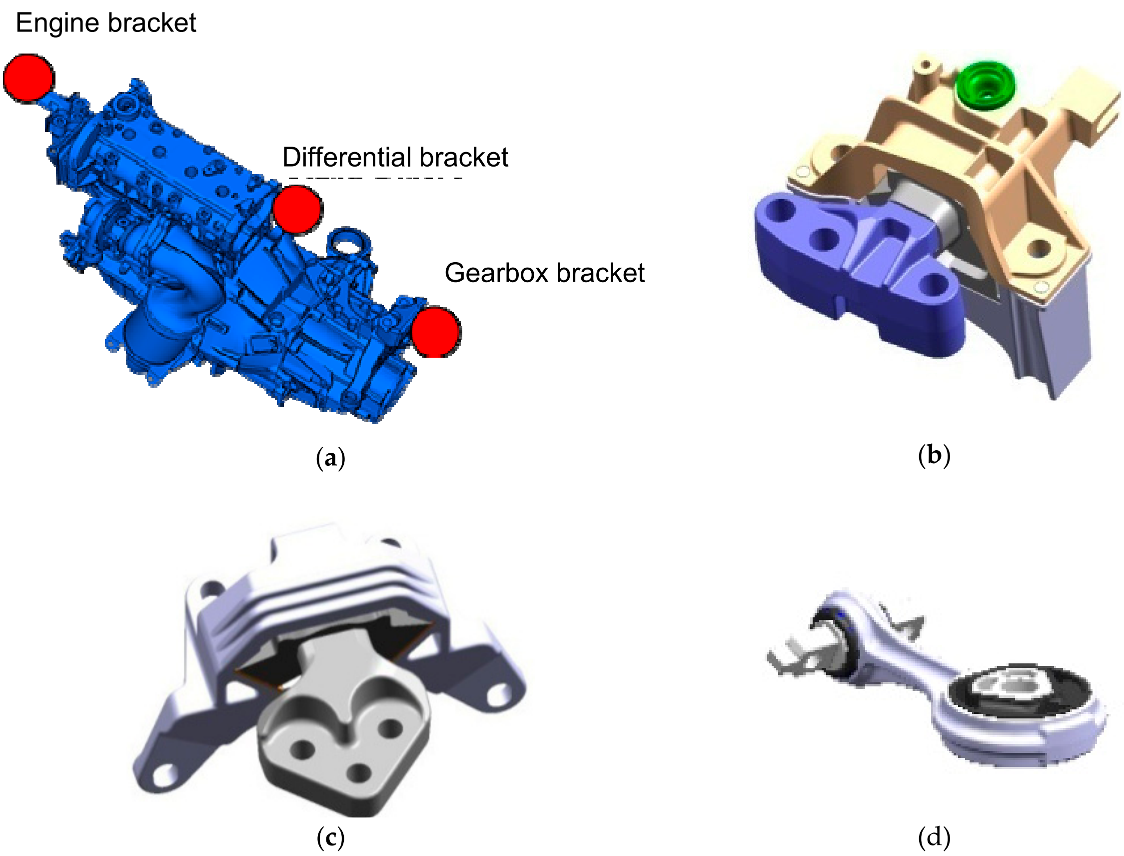

Figure 5. (**a**) Powertrain with highlight of support positions: (**b**) engine bracket; (**c**) gearbox bracket; (**d**) differential bracket.

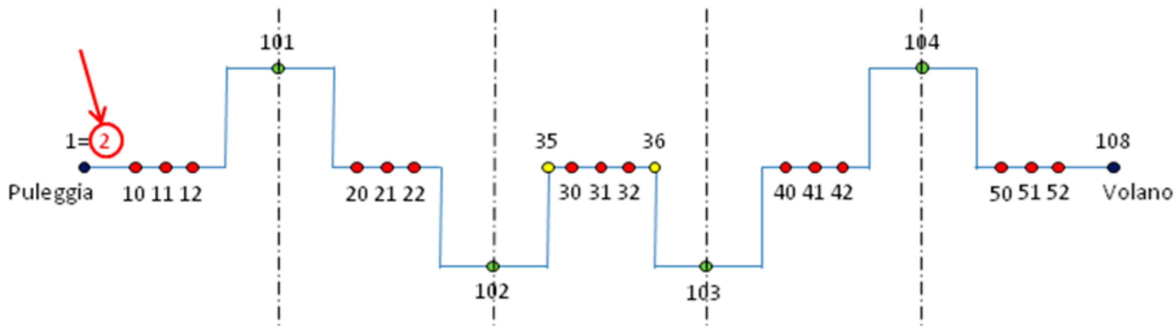

Figure 6. Highlight of added point N.2, geometrically coincident with the N.1 but rigidly connected to the seismic mass.

For all three models, the remaining powertrain components were considered as rigid, with assigned characteristics such as weight, mass center position and inertia. The gearbox was not modelled, and neither was present in the experimental bench test where an engine brake was adopted.

Therefore, the purpose of model SOL1 is purely methodological, while models SOL2 an SOL3 are those on which the analysis of interest and outcomes comparison was carried out.

2.2.1. Model SOL1

For model SOL1 some components were schematized by an appropriate rigid body, such as: crankshaft, pulley, flywheel, clutch, conrods, pistons, piston pins and rings, and power unit (base, head, oil pan, distribution components and accessories). In these cases, the specification of geometric characteristics, values of inertia, mass and position of the centers of gravity was sufficient.

Moreover, the chassis was schematized by means of a Generic Body that represents the car chassis and can be considered as a constraint on the ground to which the powertrain must be clamped by three brackets: the engine, gearbox and differential brackets.

In order to represent the constraints between adjacent bodies, appropriate joints were used. In case of bearings, they were modelled by a revolution joint, with given spring stiffness (related to the bearing stiffness) and damping value (related to oil meatus characteristics). The stiffness values of the bearings were available from AVL database and selected for the specific engine version based on in house experience. The crankshaft was connected to the crankcase by means of Revolute Joints that simulate the presence of the main bearings; this type of constraint allows to recreate a linear contact between the two bodies connected by a spring-damper modeling. In particular, the value of the clearance between shaft and crankcase and the stiffness and damping of the spring-damper system are inserted: these values, appropriately determined, depend on the maximum pressure in the combustion chamber, the bore and the maximum force discharged on the single main bearings.

No modeling of the oil meatus was provided, namely hydrodynamics of the fluid in the main bearings (e.g. between piston and cylinder liner and the conrod) was not considered. Actually, in the literature it is proposed to take into account even the elasto-hydrodynamic interactions for some applications, because, for vibroacoustic analysis, some local modes, like those in correspondence of the bearings, can play an important role, especially when considering the crankshaft bending behavior, but in this work the attention was solely focused on the shaft torsional behavior.

The axial thrust bearings, which are applied in all engines to counteract the axial thrusts generated during motion, were schematized with the constraint Axial Thrust Bearing; also in this case clearance, stiffness and damping values were included. The axial thrusts are, however, considerably lower than those deriving from the vertical thrust, generated in the combustion chamber and acting on the main bearings (with this constraint, it was possible to connect a node of the shaft to more nodes of the crankcase).

The conrods were connected to the power unit through two constraints: the first component was a prismatic guide schematized through the Piston-Liner Guidance constraint and served to

Preprints (www.preprints.org) | NOT PEER-REVIEWED | Posted: 16 May 2018 doi:10.20944/preprints201805.0223.v1

Peer-reviewed version available at *Appl. Sci.* **2018**, *8*, 1192; doi:10.3390/app8071192

simulate the constraint between rods and plungers, the second component simulated the conrod bearing, for which the joint used for main bearings was taken into consideration.

The presented modeling does not calculate the torsional critical speeds, since the motion of this calculation model is rigid, and therefore it is a zero-pulse model; as a consequence, the elements making up the system will not deform and all of them will rotate at the same speed.

2.2.2. Model SOL2

Model SOL2, introducing flexibility in the crankshaft, causes a different dynamic behavior of the system and allows to evaluate those critical torsional speeds non-visible in model SOL1. This element of flexibility was introduced into the calculation model through an FE modeling of the body crankshaft.

Modal analyses were performed in shaft free – free conditions in order to obtain the system eigenmodes of vibration with their eigenfrequencies. In such a model (Fig. 7) the clutch unit was modeled as a concentrated mass. In Figure 8 the FE models of flywheel and pulley are shown.

The adopted mesh is based on tetrahedral elements with element average size equal to 0.5 mm.

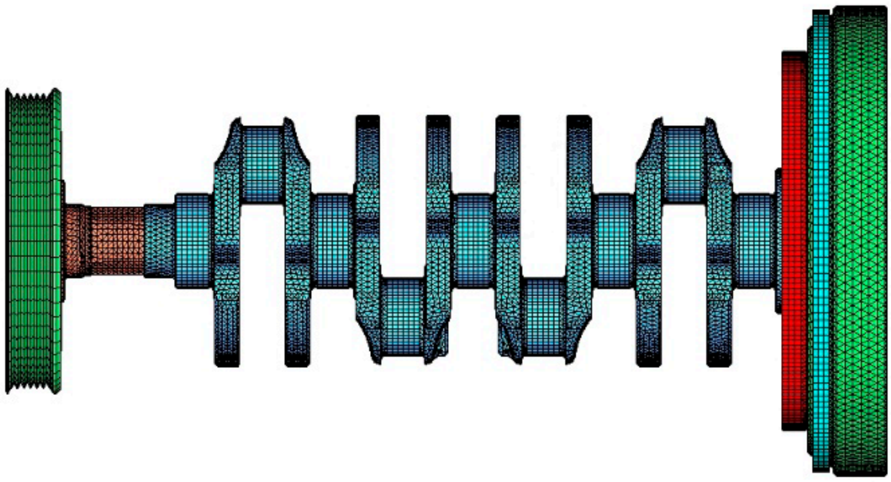

Figure 7. FE model of the shaft with clutch mechanism modelled as a concentrated mass.

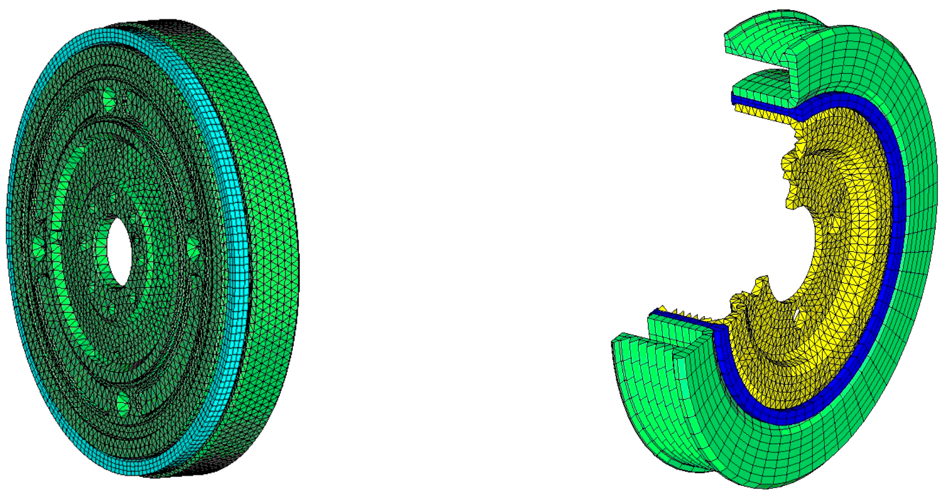

(**a**) (**b**)

Figure 8. FE model of the flywheel (**a**) and pulley (**b**).

2.2.3. Model SOL3

In addition to considering the flexibility of the crankshaft, model SOL3 was provided with the FE modeling of the clutch mechanism (Fig. 9).

The crankshaft mesh, with FE modeled clutch mechanism, included about 450,000 tetrahedral and hexahedral elements and about 140,000 nodes. In table 1 the salient features of the three models, SOL1, SOL2 and SOL3, are also shown.

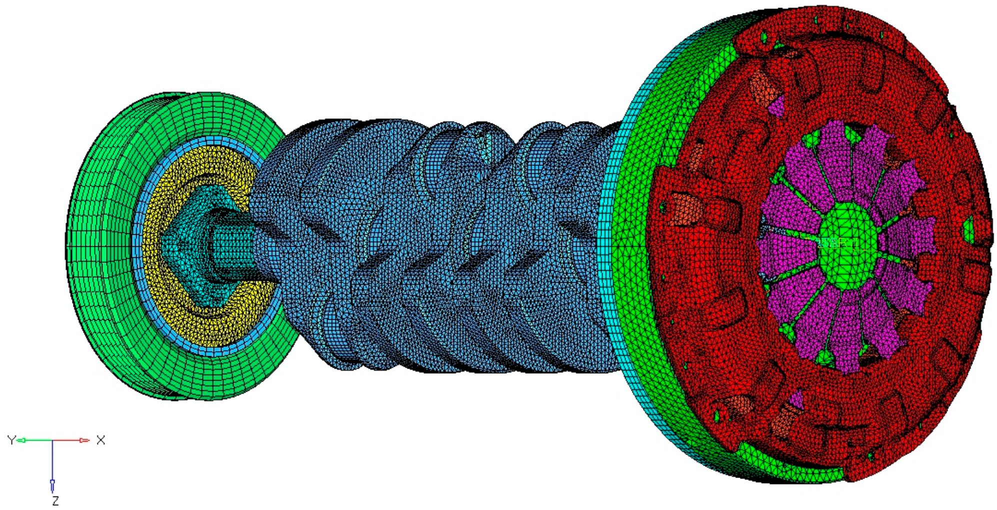

Figure 9. FE model of the shaft with discretized clutch mechanism.

Table 1. Characteristics of the calculation models.

MODEL	AVL/EXCITE ELEMENTS USED FOR THE SCHEMATISATION	MODELED FE ELEMENTS	PURPOSE
SOL1	CRANKSHAFT, CONROD, POWERUNIT, GENERIC BODY, REVOLUTE JOINT, AXIAL THRUST BEARING, PISTON-LINER GUIDANCE, TABLE FORCE/MOMENT	-	PROCEDURAL – FOR THE VERIFICATION OF THE NEXT STEPS
SOL2	CONROD, POWERUNIT, GENERIC BODY, REVOLUTE JOINT, AXIAL THRUST BEARING, PISTON-LINER GUIDANCE, TABLE FORCE/MOMENT	CRANKSHAFT, PULLEY, FLYWHEEL	ANALYSIS AND COMPARISON
SOL3	CONROD, POWERUNIT, GENERIC BODY, REVOLUTE JOINT, AXIAL THRUST BEARING, PISTON-LINER GUIDANCE, TABLE FORCE/MOMENT	CRANKSHAFT, PULLEY, FLYWHEEL, CLUTCH MECHANISM	ANALYSIS AND COMPARISON

2.3. Experimental setup

The experimental measurements were performed on a test bench (rather than real vehicle), considering in particular a measurement point located on the powertrain flywheel; therefore, in order to have a reliable comparison, the experimental motion irregularities are compared with the numerical ones in a reference node located in the mass center of the flywheel (node 108 as in Fig. 6). The calibration between numerical and experimental tests is based on the measured torque.

Preprints (www.preprints.org) | NOT PEER-REVIEWED | Posted: 16 May 2018 doi:10.20944/preprints201805.0223.v1

Peer-reviewed version available at Appl. Sci. 2018, 8, 1192; doi:10.3390/app8071192

3. Results

3.1. Model SOL1

Model SOL1, presenting all rigid elements, although not leading to useful outcomes regarding the determination of the critical torsional speeds, allowed to obtain important outcomes for the model verification purposes, including: motion irregularity of crankshaft and global vibration index for the brackets.

It is well known that in an internal combustion engine the engine torque generated by gas and inertia forces is periodical and subject to breakdown into Fourier series as a sum of harmonics that can be more or less relevant to the engine dynamics according to the associated amplitude, phase and order value.

3.1.1. Motion irregularities

The outcomes of the simulation obtained with a rigid crankshaft (SOL1), focus on the study of the motion irregularities detected in the center of gravity of flywheel (node 108), hub (node 1) and seismic mass (node 2) as in Figure 6.

The even orders are the most relevant for the engine torque of a 4-strokes, 4-cylinder engine, therefore, its influence should be considered for motion irregularities assessment. Consequently, an evaluation of the magnitude of the second engine order crankshaft motion irregularity vs. speed was primarily carried out on the engine under test (Fig. 10a).

The Campbell diagram represents the frequency spectrum of a non-stationary signal, in which the frequency is indicated on the axis of abscissas, the average angular velocity on the axis of ordinates and the color chart indicates the oscillation amplitude of the variable under test (in this case Δrpm): this diagram for the motion irregularity evaluated on the flywheel (Fig. 10b) clearly shows the prevalence of the 2nd engine order. It is interesting to observe that the 6th order seems to not exhibit any appreciable peak of motion irregularities, but this outcome will be invalidated when the allowance for modal behavior will be included in the analysis.

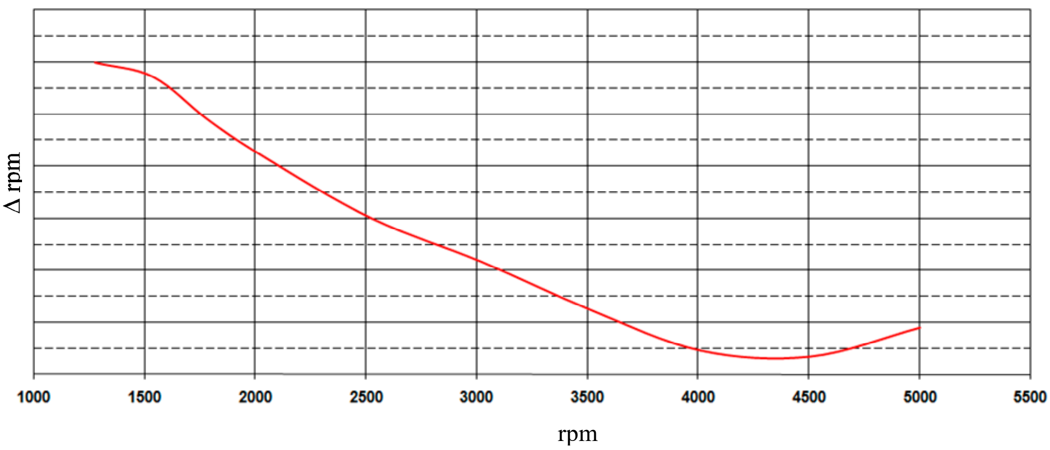

(a)

Preprints (www.preprints.org) | NOT PEER-REVIEWED | Posted: 16 May 2018 doi:10.20944/preprints201805.0223.v1

Peer-reviewed version available at *Appl. Sci.* **2018**, *8*, 1192; doi:10.3390/app8071192

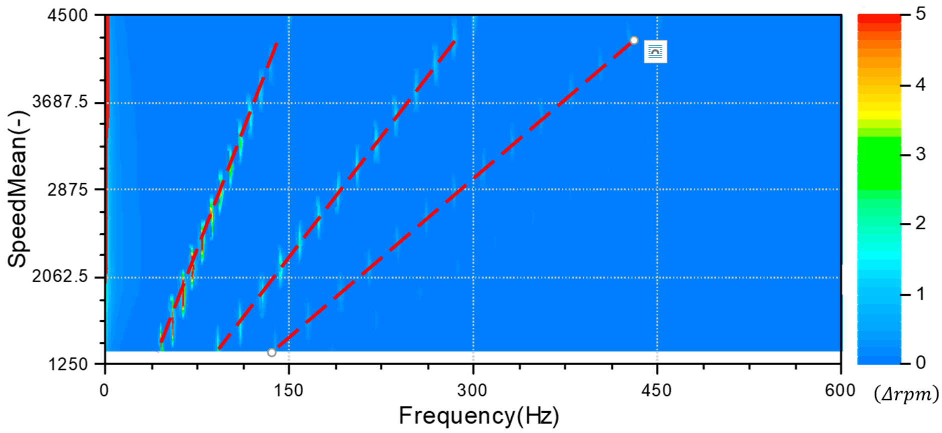

(**b**)

Figure 10. Motion irregularities - model SOL1: (**a**) 2nd engine order vs. speed and (**b**) Campbell diagram of the motion irregularities with highlight of 2nd, 4th and 6th engine orders.

3.1.2. Global vibration index

A global vibration index for the brackets, called weighted sum, was also calculated and defined as follows:

$$X(f) = \sqrt{\sum_{i=1}^{n} w_i^2(f) \cdot x_i^2(f)} \quad (1)$$

where:

wi(f) is the weighing factor for a given direction and position,
xi(f) is the rms acceleration for a given direction and position,
n is the total number of positions and directions (x, y and z) = number of brackets × 3.

The weighing factors to be used in this relation depend on the vehicle in which the powertrain must be installed and are generally provided by the vehicle platform unit. Without such information, as in our case, the coefficients are all set to 1 (uniform weighing of the structural transmission paths).

The second order of the global vibration index of each bracket (engine, gearbox and differential brackets) is shown in Figure 11: e.g. showing a contribution that is nearly frequency independent for gear box and differential brackets, whereas it turns out to be increasing with frequency when considering the engine bracket. The corresponding global vibration index is shown in Figure 12 with reference to the amplitudes of numerical and experimental acceleration irregularities, and therefore to the amount of the transmitted vibration.

Preprints (www.preprints.org) | NOT PEER-REVIEWED | Posted: 16 May 2018 doi:10.20944/preprints201805.0223.v1

Peer-reviewed version available at Appl. Sci. 2018, 8, 1192; doi:10.3390/app8071192

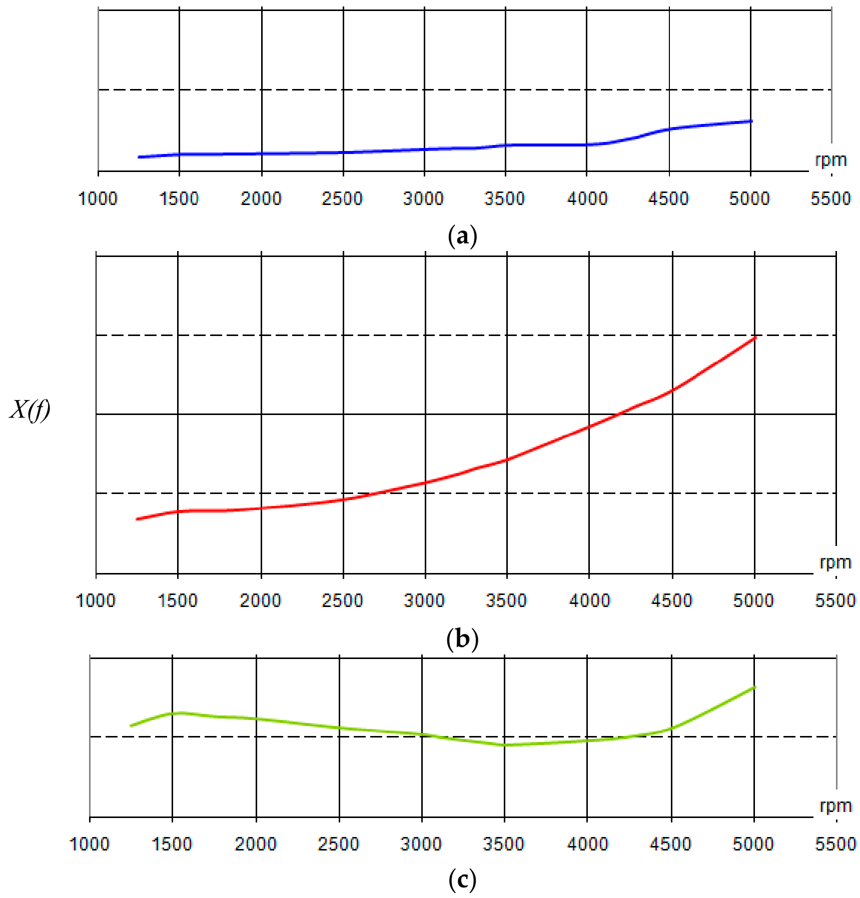

Figure 11. Numerical bracket vibration indexes *X(f)* [m/s²] for the second engine order: (**a**) gear box; (**b**) engine; (**c**) differential.

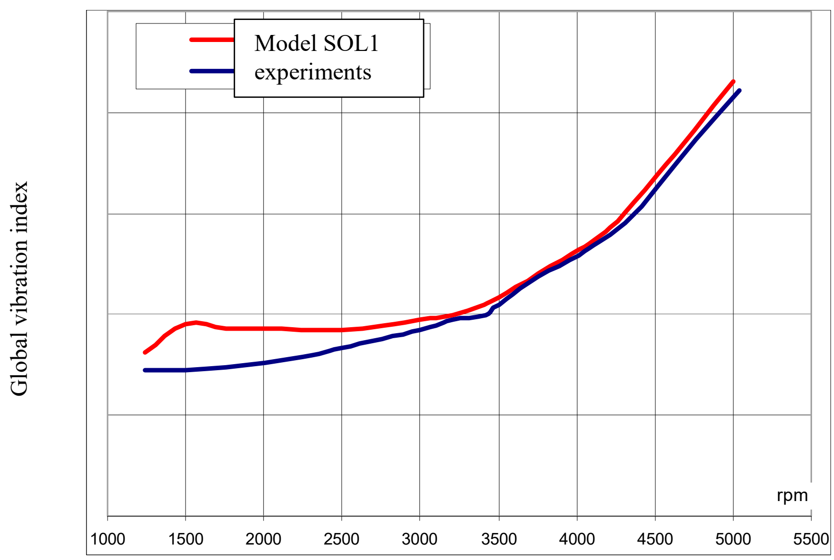

Figure 12. Numerical-experimental comparison of the brackets global vibration index for the second engine order.

Model SOL1 allows to verify some operating parameters, such as the motion irregularities and the global vibration index for the brackets, and it also allows to highlight that, as expected, the second engine order harmonic force is predominant when neglecting flexibility of any component.

Preprints (www.preprints.org) | NOT PEER-REVIEWED | Posted: 16 May 2018 doi:10.20944/preprints201805.0223.v1

Peer-reviewed version available at *Appl. Sci.* **2018**, *8*, 1192; doi:10.3390/app8071192

3.2. Model SOL2

3.2.1. Motion irregularities

From the modal analysis it is possible to observe that, for the engine under test in its operating range, the first two torsional modes are respectively at 305 and 545 Hz (Fig. 13): in the former the hub and the seismic mass oscillate in phase whereas in the latter their oscillation is out of phase.

The primary objective here is to detect how the amplitude of the motion irregularities are affected by the shaft torsional eigenfrequencies: in fact, in correspondence of resonances, the irregularities may take values so high to make them critical to the vibro-acoustic behavior of the whole powertrain.

The outcomes of model SOL2 are compared with the test evaluations in order to assess the accuracy of the used calculation model; considering that the experimental measurements are only available on the flywheel center, the numerical–experimental comparison can only involve node 108 (Fig. 6).

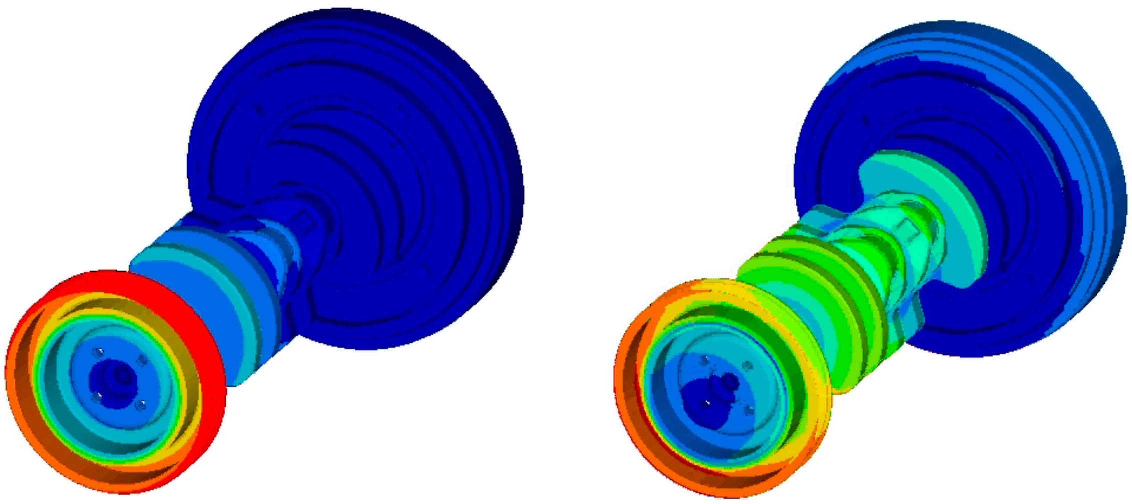

(**a**) (**b**)

Figure 13. 1st (**a**) and 2nd (**b**) torsional eigenmodes at respectively 305 and 545 Hz.

The 2nd order of motion irregularity does not display any peak in the range 1250-5000 rpm (Fig. 14) and this is expected since the maximum involved excitation frequency,

$$f = 2*5000/60 = 166.7\ Hz,$$

is not sufficiently high to trigger the first torsional eigenmode at 305 Hz; consequently, SOL 2 provide the same results of SOL 1 and a satisfactory correlation with experimental measurements made at flywheel (node 108), as in Figure 15. The minimum of the motion irregularities is at nearly 4250 rpm: in correspondence of such regime the combustion forces and inertia forces are almost in equilibrium.

Preprints (www.preprints.org) | NOT PEER-REVIEWED | Posted: 16 May 2018 doi:10.20944/preprints201805.0223.v1

Peer-reviewed version available at *Appl. Sci.* **2018**, *8*, 1192; doi:10.3390/app8071192

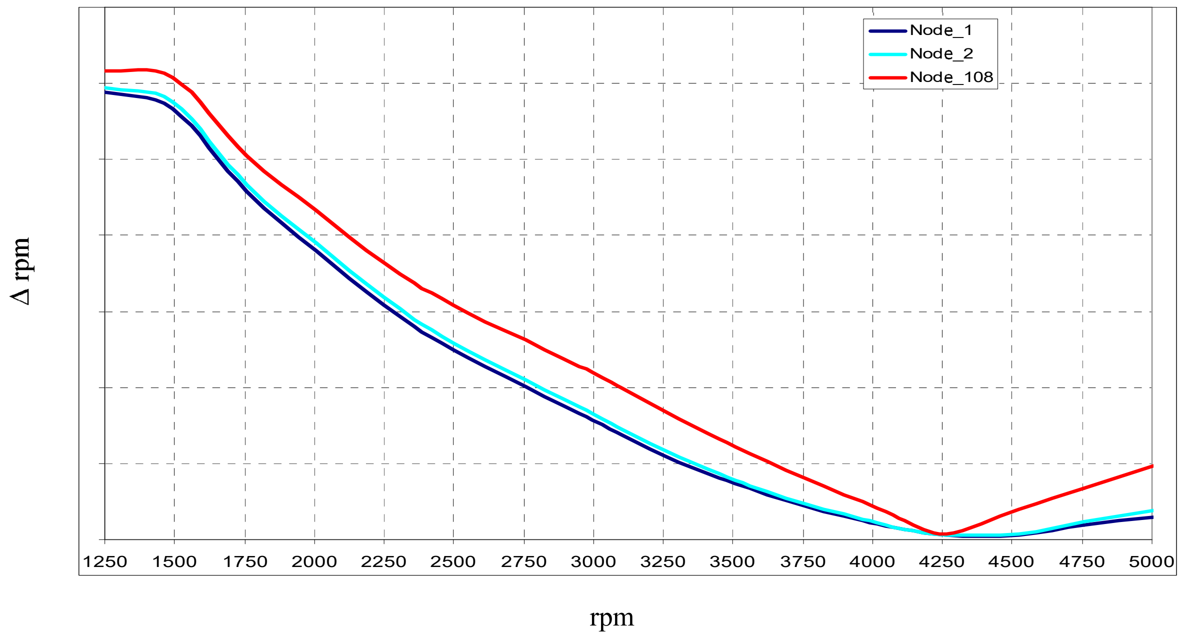

Figure 14. Numerical motion irregularities for the 2[th] engine order at nodes 1, 2 and 108, as provided by model SOL2.

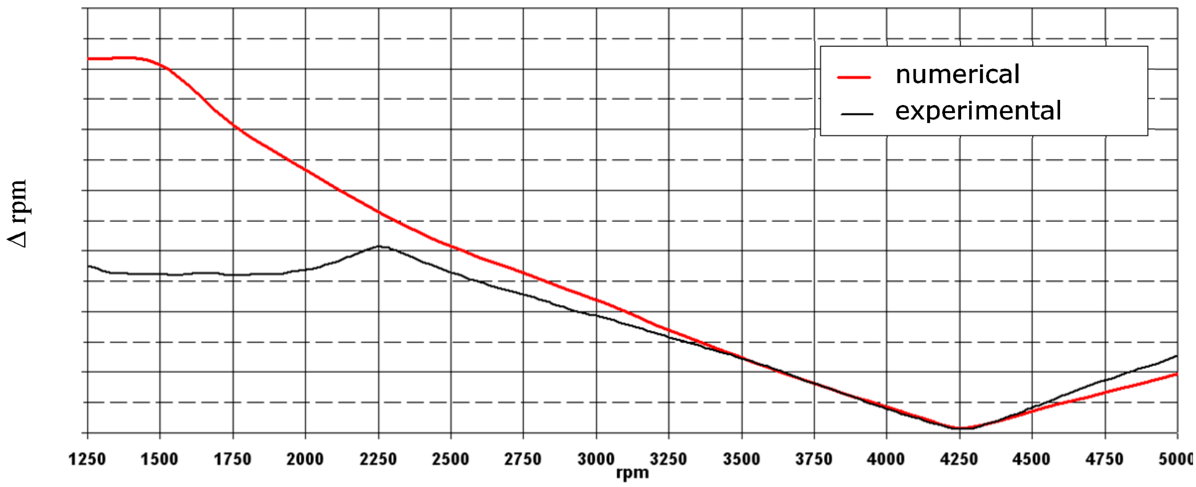

Figure 15. Numerical-experimental comparison of the motion irregularities for the 2[nd] engine order at node 108.

On the contrary, the 4[th] order of motion irregularity does display a peak in the range 1250-5000 rpm at nearly 4500 rpm (Fig. 16), in correspondence of a frequency

$$f = 4*4500/60 = 300\ Hz,$$

that is sufficiently close to the 1st torsional eigenfrequency (305 Hz) to confirm the hypothesis of a resonant behavior for the crankshaft. Such peak manifests only with reference to nodes 1 and 2 but is negligible for node 108 (Fig. 16).

A good correspondence between numerical and experimental results is provided by SOL2 (Fig. 17) for regimes higher than 2000 rpm, even if a slight underestimation of the irregularities is obtained. The lack of numerical vs. experimental correlation at low regimes is expected due to the turbolag phenomenon: during the bench test, based on an acceleration from the min to the max regime, the turbo does not properly work at low regime (lower than 2000 rpm) whereas the simulation cannot allow for such drawback being based on a quasi-stationary variation of loading conditions.

It is worth to point out that, as expected, the amplitude of oscillation for node 2 is higher than that of node 1: as a matter of fact, hub and seismic mass oscillate in phase, with the latter being more peripheral and consequently with larger oscillations.

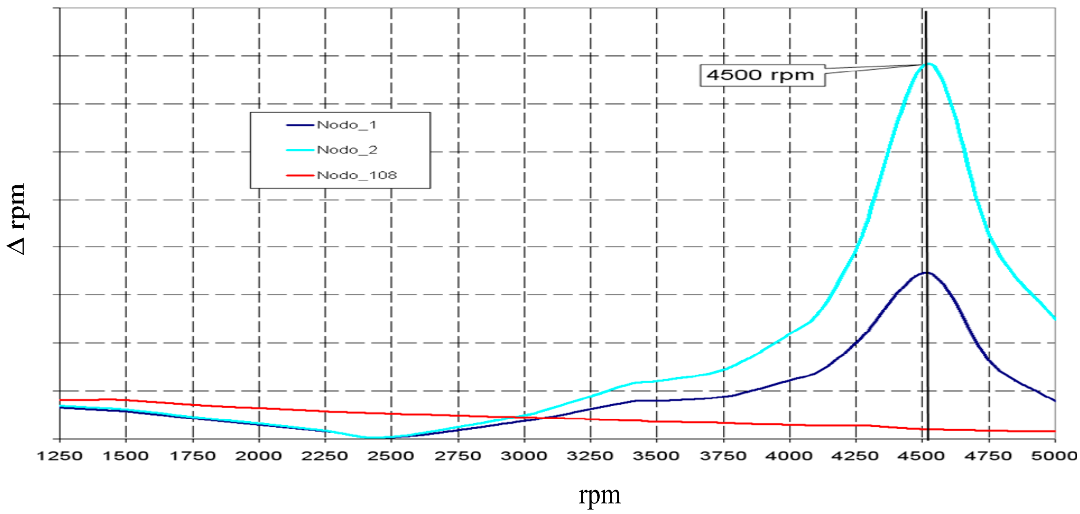

Figure 16. Numerical motion irregularities for the 4th engine order at nodes 1, 2 and 108, as provided by model SOL2.

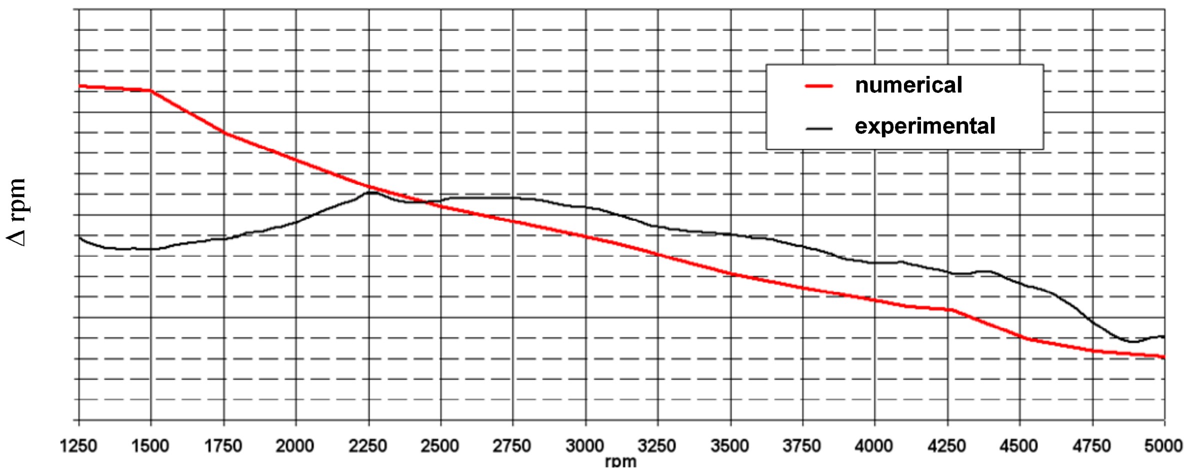

Figure 17. Numerical-experimental comparison of the motion irregularities for the 4th engine order at node 108, as provided by model SOL2.

Exploring now the 6th order we can see a numerical peak at nearly 3050 rpm [18], in correspondence of a frequency

$$f = 6*3050/60 = 305\ Hz,$$

that, again, being coincident with the 1st torsional eigenfrequency (305 Hz) confirms the hypothesis of a resonant behavior for the crankshaft.

This time, apart from the discrepancies at the low regimes affected by the turbolag phenomena, a non-negligible underestimation of motion irregularities provided by the simulation is coming out also at higher regimes (Fig. 19): this might be due to the fact that the only crankshaft is modelled with allowance for its flexibility. Moreover, the experimental peak is at 3100 rpm whereas the numerical peak is at 3050 rpm (Fig. 18), but this discrepancy can be due to approximations in the "discrete" acquisition procedure.

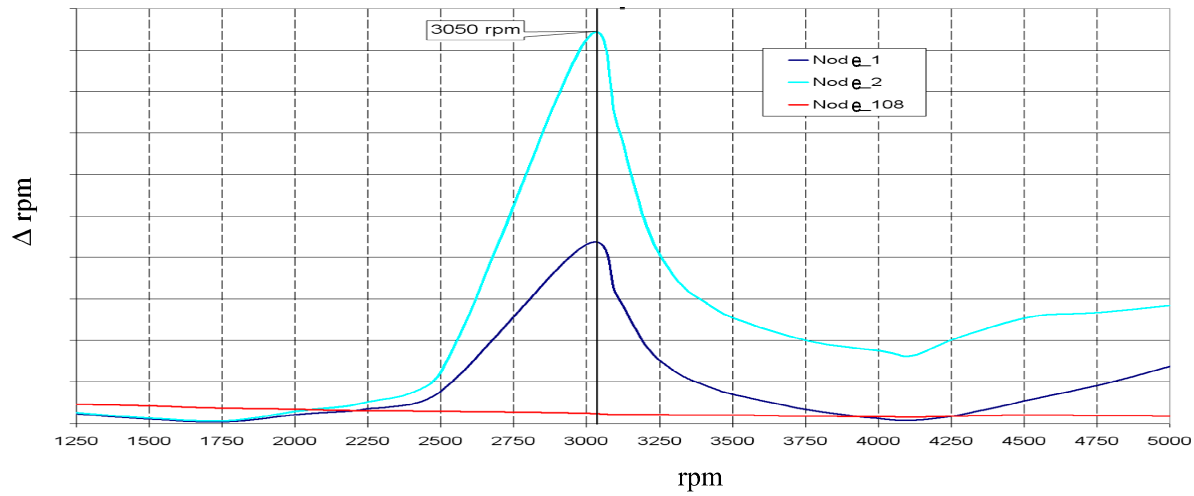

Figure 18. Numerical motion irregularities for the 6th engine order at nodes 1, 2 and 108, as provided by model SOL2.

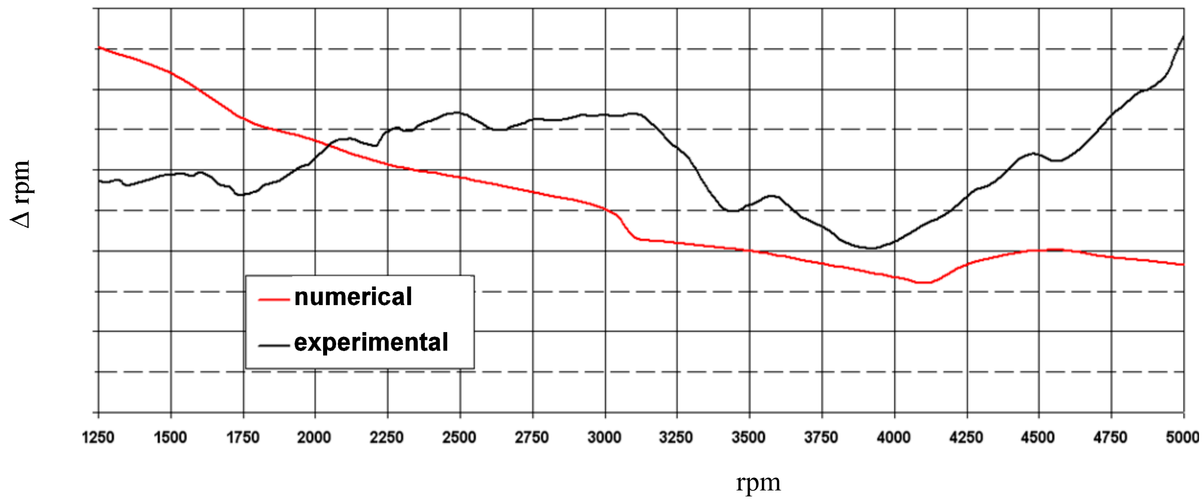

Figure 19. Numerical-experimental comparison of the motion irregularities for the 6th engine order at node 108, as provided by model SOL2.

Exploring now the 8th order we can see two peaks at nearly 2250 and 4250 rpm (Fig. 20), respectively in correspondence of the frequencies

$$f_1 = 8*2250/60 = 300\ Hz,$$

$$f_2 = 8*4250/60 = 567\ Hz,$$

that are sufficiently close to the 1st (305 Hz) and 2nd (545 Hz) torsional eigenfrequencies to confirm the hypothesis of resonant behavior for the crankshaft (Fig. 20).

Again, a slight underestimation of motion irregularities provided by the simulation is evident (Fig. 21).

Peer-reviewed version available at Appl. Sci. 2018, 8, 1192; doi:10.3390/app8071192

In conclusion, the 2nd torsional eigenfrequency cannot be triggered by orders lower than the 8th; moreover, orders higher than the 8th are neglected because their amplitude is sufficiently low to prevent a relevant impact when triggering the torsional eigenfrequencies.

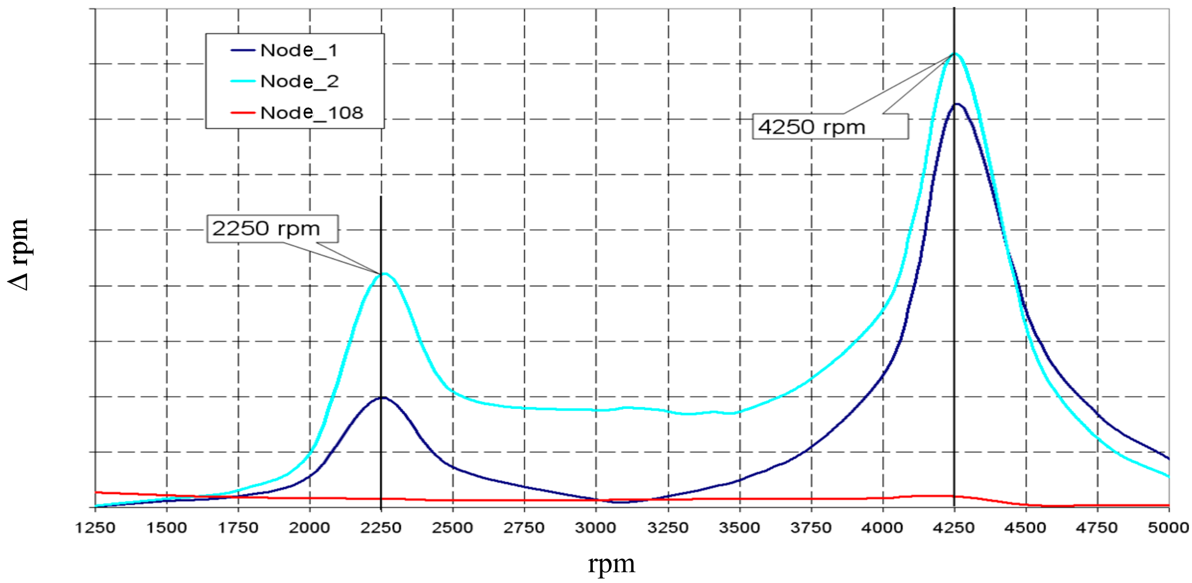

Figure 20. Numerical motion irregularities for the 8th engine order at nodes 1, 2 and 108, as provided by model SOL2.

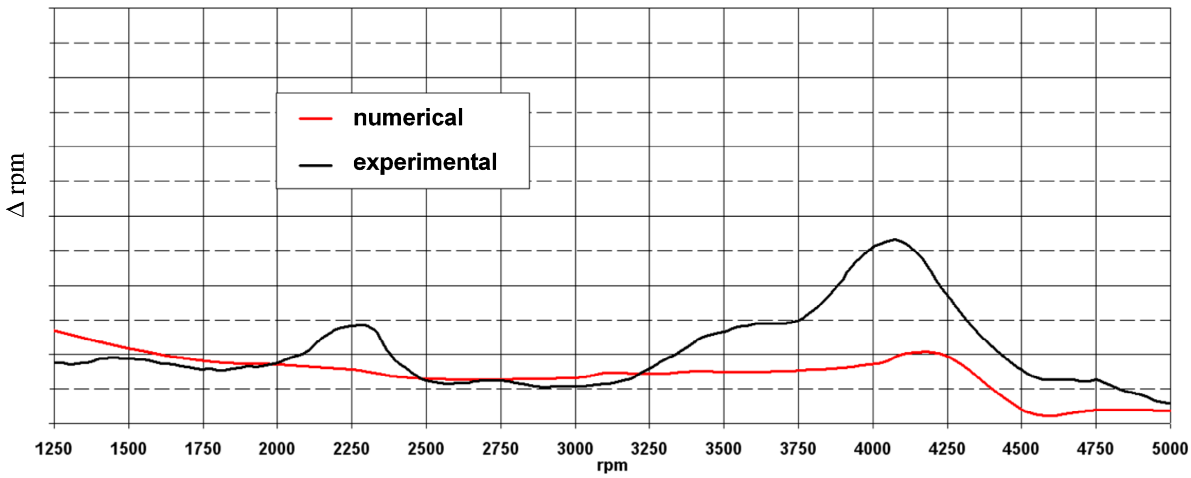

Figure 21. Numerical-experimental comparison of the motion irregularities for the 8th engine order at node 108, as provided by model SOL2.

3.3. Model SOL3

For what concerns model SOL3 the outcomes of the 2nd engine orders motion irregularities do not differ significantly from those observed in model SOL2. In contrast, for what concerns the 4th engine order, different outcomes between the two models are recorded (Fig. 22). In particular, a different trend of the brackets vibrations due to the explicit FE modelling of the clutch mechanism is observed.

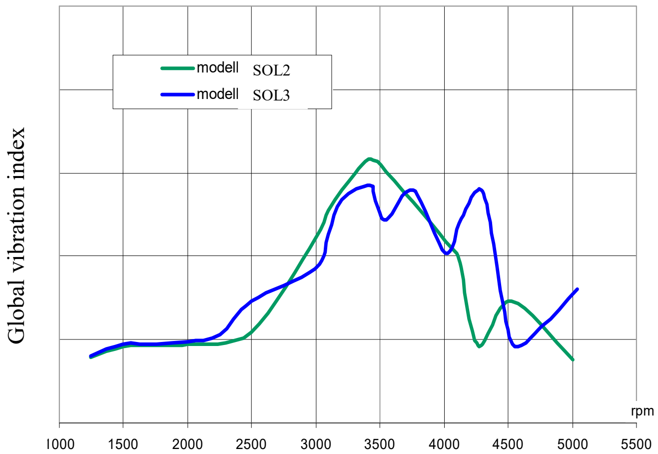

Figure 22. Global vibration index for the 4th engine order brackets: comparison between models SOL2 and SOL3.

4. Conclusions

In this work three internal combustion turbocharged diesel engine multibody models of increasing complexity were developed and their vibration behavior observed.

The development of the multibody models allows to analyze the support brackets vibrations, in order to proceeds to a design optimization solution in production and\or development phase. The observed outcomes of the three analyzed models provide the following conclusions:

- for what concerns the 2nd engine order motion irregularities and global vibration index, the rigid body model shows a good correlation with the experimental outcomes;
- the flexible shaft model shows an adequate degree of correlation for the 2nd and 4th engine order motion irregularities; such model represents the best compromise between computational speed and calculation accuracy and provides also outcomes which can be used for analyses requiring a more in-depth study;
- the flexible shaft and clutch mechanism FE model allows a further degree of analysis as gives the possibility to improve the outcomes related to the 4th engine order support brackets vibrations.

Peer-reviewed version available at *Appl. Sci.* **2018**, *8*, 1192; doi:10.3390/app8071192

References

1. Citarella, R.; Federico, L. Advances in Vibroacoustics and Aeroacustics of Aerospace and Automotive Systems. *Appl. Sci.* **2018**, *8*, 366; DOI: 10.3390/app8030366.
2. Bianco, D.; Adamo, F.P.; Barbarino, M.; Vitiello, P.; Bartoccini, D.; Federico, L.; Citarella, R. Integrated Aero–Vibroacoustics: The Design Verification Process of Vega-C Launcher. *Appl. Sci.* **2018**, *8*, 88; DOI: 10.3390/app8010088.
3. Armentani, E.; Sbarbati, F.; Perrella, M.; Citarella, R. Dynamic analysis of a car engine valve train system. *Int. J. of Vehicle Noise and Vibration* **2016**, *12*, 229–240, DOI: 10.1504/IJVNV.2016.080138.
4. Yakoub, R.Y.; Corrado, M.; Forcelli, A.; Pappalardo, T.; Dutre, S. Prediction of System-Level Gear Rattle Using Multibody and Vibro-Acoustic Techniques. *SAE Technical Paper* **2004**, DOI: 10.4271/2004-32-0063.
5. Gérard, F.; Tournour, M.; El Masri, N.; Cremers, L.; Felice, M.; Selmane, A. Acoustic Transfer Vectors for Numerical Modeling of Engine Noise, *Sound and Vibration Magazine* **2002**, *36*, 20-24.
6. Citarella, R.; Federico, L.; Cicatiello, A. Modal acoustic transfer vector approach in a FEM–BEM vibro-acoustic analysis. *Engineering Analysis with Boundary Elements* **2007,** *31*, 248–258, DOI: 10.1016/j.enganabound.2006.09.004.
7. Gustafsson, M.; Jacqmot, J.; Caro, S. Experimental Validation of an Efficient Procedure for Large Acoustic Radiation Problems, Proceedings of ISMA2010 including USD2010, 2010, pp. 4557-4566, ISBN: 978-907380287-2.
8. Armentani, E.; Sepe, R.; Parente A.; Pirelli, M.; Vibro-Acoustic Numerical Analysis for the Chain Cover of a Car Engine, *Appl. Sci.* **2017**, 7, 610, DOI: 10.3390/app7060610.
9. Hua, X.; Lim, T.C.; Peng, T.; Wali, W.E. Dynamic Analysis of Spiral Bevel Geared Rotor Systems Applying Finite Elements and Enhanced Lumped Parameters. *Int.J Automot. Technol.* **2012**, *13*, 97-107, DOI: 10.1007/s12239-012-0009-4.
10. Hua, X.; Lim, T.; Peng, T. Effect of Shaft-bearing Configurations on Spiral Bevel Gear Mesh and Dynamics. *SAE Technical Paper* **2011**, DOI: 10.4271/2011-01-1551.
11. Xu, X.; Luo, T.; Luo, J.; Hua, X.; Langari R. Dynamical load sharing behaviors of heavy load planetary gear system with multi-floating components. *International Journal of Modeling, Simulation, and Scientific Computing* **2018**, *9*, 1, DOI: 10.1142/S1793962318500058.
12. Hanim, S.; Zouani, A.; Felice, M. Integrated dynamic engine simulation for automotive noise & vibration predictions, NAFEMS Americas conference, 2016.
13. Östman, F.; Toivonen, H.T. Adaptive Cylinder Balancing of Internal Combustion Engines. *IEEE Transactions on Control Systems Technology* **2011,** *19*, 4, 782–791, DOI: 10.1109/TCST.2010.2052925.
14. Giakoumis, E.G.; Rakopoulos, C.D.; Dimaratos, A.M. Study of crankshaft torsional deformation under steady-state and transient operation of turbocharged diesel engines. Proceedings of the I MECH E, Part K: *Journal of Multi-body Dynamics* **2008**, *222*, 1, 17-30, doi:10.1243/14644193jmbd113.
15. Offner, G.; Priebsch, H.; Elastic body contact simulation for predicting piston slap induced noise in an IC engine, in: H. Rahnejat, M. Ebrahimi, R. Whalley (Eds.), Multi-Body Dynamics: Monitoring and Simulation Techniques-II, 191-206. Professional Engineering Publishing, London (2000).
16. Offner, G.; Krasser, J.; Laback, O.; Priebsch, H. Simulation of multi-body dynamics and elastohydrodynamic excitation in engines especially considering piston-liner contact, Proceedings of the Institution of Mechanical Engineers, Part K: *Journal of Multi-body Dynamics* **2001**, *215*, 93-102, DOI: 10.1243/1464419011544385.
17. Junhong, Z.; Jun, H. CAE process to simulate and optimise engine noise and vibration, *Mechanical Systems and Signal Processing* **2006**, *20*, 1400-1409, DOI: 10.1016/j.ymssp.2004.11.005
18. Gawande, S. H.; Navale, L. G.; Nandgaonkar, M. R.; Butala, D. S.; Kunamalla, S. Fault Detection of Inline Reciprocating Diesel Engine: A Mass and Gas-Torque Approach, *Advances in Acoustics and Vibration*, **2012**, 1-6, doi:10.1155/2012/314706.
19. Siano, D.; Citarella, R. Elastic Multi Body Simulation of a Multi-Cylinder Engine. *The Open Mechanical Engineering Journal* **2014**, *8*, 157-169, DOI: 10.2174/1874155X01408010157.
20. Siano, D.; Citarella, R.; Armentani, E. Simulation of a multi-cylinder engine vibrational behaviour, *Int. J. Vehicle Noise and Vibration* **2018** (in press).
21. Dassault Systems Simulia Corp., Abaqus Analysis User's Manual, Version 6.12.1, Providence, RI, USA, (2011).
22. AVL EXCITE Base Module Reference Manual.

23. Kim, S.J.; Kim, S.G.; Oh, K.S.; Lee, S.K. Excitation Force Analysis of a Powertrain Based on CAE Technology. *International Journal of Automotive Technology* **2008**, 9(6), 703-711, DOI: 10.1007/s12239-008-0083-9.
24. Craig, R..; Bampton, M. Coupling of Substructures for Dynamic Analyses. *AIAA Journal*, American Institute of Aeronautics and Astronautics **1968**, *6* (7), 1313-1319.
25. Armentani, E.; Trapani, R.; Citarella, R.; Parente, A.; Pirelli, M.; FEM-BEM Numerical Procedure for Insertion Loss Assessment of an Engine Beauty Cover. The Open Mechanical Engineering Journal **2013**, *7*, 27-34, DOI: 10.2174/1874155X01307010027.